ChemPubSoc
Europe

FULL PAPER

Growth and Characterization of Centimeter-Sized Ba$_2$LaFeNb$_4$O$_{15}$ Crystals from High-Temperature Solution under a Controlled Atmosphere

Marjorie Albino,[a] Philippe Veber,[a] Elias Castel,[b][‡] Matias Velázquez,[a] Kurt Schenk,[b] Gervais Chapuis,[b] Michel Lahaye,[a] Stanislav Pechev,[a] Mario Maglione,[a] and Michaël Josse*[a]

Centimeter-sized single crystals of Ba$_2$LaFeNb$_4$O$_{15}$ were grown from a high-temperature solution by using LiBO$_2$ flux and a sealed platinum assembly. The obtained single crystals display the same physical properties as their ceramic counterparts. A frequency-dependent dielectric permittivity maximum was found (T_m = 100 K at 5 kHz), which indicates relaxor behavior. Magnetic susceptibility measurements revealed purely paramagnetic behavior between 10 and 350 K. X-ray diffraction measurements of Ba$_2$LaFeNb$_4$O$_{15}$ single crystals revealed an incommensurate structure at room temperature with a bidimensional modulation characterized by vectors $q_1 = (a, a, 1/2)$ and $q_2 = (a, -a, 1/2)$ with $\alpha = 0.295(1)$. This crystal growth method offers a promising elaboration route to centimeter-sized crystals of niobate-based compounds, which may not be grown from the pure liquid phase, especially those with a tetragonal tungsten bronze (TTB) structure.

Introduction

Materials with the tetragonal tungsten bronze (TTB) crystal structure can display a large variety of physical properties depending on their chemical composition; these include photoelectrochemical properties,[1] properties suitable for use as solid oxide fuel cell anodes,[2–5] nonlinear dielectric behavior, and piezoelectric, pyroelectric, ferroelectric, and relaxor responses.[6] For these latter properties, TTB niobates are particularly relevant, owing to the "ferroelectrically active" nature of the Nb^{5+} ions. The general formula of TTB-type materials may be written as A$_2$BC$_2$M$_5$O$_{15}$, in which the A sites contain large ions such as alkali and alkaline-earth ions, the B sites can contain rare-earth ions, and the octahedral M sites accommodate cations such as Ti^{4+}, Nb^{5+}, and Ta^{5+}. The C sites are usually empty in ferroelectric TTB materials with the notable exception of K$_3$Li$_2$Nb$_5$O$_{15}$. The presence of crystallographi-

cally nonequivalent A, B, and M sites, and an extra C site provide additional degrees of freedom with respect to perovskites, for example, for the manipulation of the crystal structure, and hence these materials offer huge compositional flexibility.[7]

The most widely studied members of this family are barium sodium niobate Ba$_2$NaNb$_5$O$_{15}$ (BNN), the archetype of TTB ferroelectrics, which displays interesting nonlinear optical, electro-optical, and piezoelectric properties. Many studies of these materials in single-crystal form can be found in the literature. Several deal with pure and rare-earth doped BNN growth experiments performed by the Czochralski technique.[8–23] Microtwins, related to the orthorhombic structure of BNN, and cracks caused by thermal expansion along the c axis in the ferroelectric phase transition[14,24] are observed in such crystals. Crystalline fibers grown by the laser-heated pedestal growth (LHPG)[25–29] and the micro-pulling-down technique (μ-PD)[30–33] do not suffer such formation of cracks and twins. These growth techniques can produce high quality BNN crystals of limited size (below 1 mm diameter). Since 2006, the optical properties of BNN single crystals (with sizes up to $2 \times 2 \times 3$ mm^3) activated with trivalent lanthanide ions and grown in Na$_2$B$_4$O$_7$ flux have been examined.[34–36]

Structural features play a crucial role in the physical properties of TTB niobates, especially their dielectric properties. In the paraelectric state, the TTB structure is expected to be centrosymmetric with space group P4/*mbm*.[37]

___
[a] CNRS, Université de Bordeaux, ICMCB,
   87 avenue du Dr. A. Schweitzer, 33608 Pessac cedex, France
   Fax: +33-5-40002761
   E-mail: josse@icmcb-bordeaux.cnrs.fr
   Homepage: http://www.icmcb-bordeaux.cnrs.fr
[b] Laboratoire de Cristallographie, Ecole Polytechnique Fédérale de Lausanne (EPFL),
   BSP - Cubotron, 1015 Lausanne, Switzerland
[‡] Current address: Paul Scherrer Institut, Electrochemistry Laboratory,
   5232 PSI Villigen, Switzerland
   Supporting information for this article is available on the WWW under http://dx.doi.org/10.1002/ejic.201300008.

WILEY
ONLINE LIBRARY

www.eurjic.org   **FULL PAPER**

In the polar state, dipolar moments are usually induced by displacements of niobium ions along the *c* axis within their octahedral sites to yield a structural description in the noncentrosymmetric space group *P4bm*. Although early structural investigations on BNN[38–41] and $Sr_{1−x}Ba_xNb_2O_6$ (SBN)[42–43] proposed a commensurate model for the crystalline structure of these TTB niobates, some structural subtleties were also pointed out (barium position splitting, octahedral tiltings).

Schneck et al.[44] and Labbe et al.[45] revealed the incommensurate character of the crystal structure of SBN, which is similar to the previously discovered incommensurability in BNN[46] and appears in combination with ferroelastic properties.[47] Simon et al.[48] showed that SBN crystals exhibit anisotropic dielectric behavior. They behave as relaxors along the [001] direction and as ferroelectrics along the [100] direction; such features are possibly related to the existence of structural modulations. Recently, the incommensurate structure of SBN was solved and refined as a five dimensional (5D) modulated structure in the superspace formalism.[49] In 2012, Graetsch et al.[50–51] obtained single crystals of undoped $Ca_{0.28}Ba_{0.72}Nb_2O_6$ and cerium-doped $Ce_{0.02}Ca_{0.25}Ba_{0.72}Nb_2O_6$, which also displayed an incommensurately modulated TTB structure describable in a 5D superspace.

In addition, several TTB materials revealed different dielectric properties depending on the modification of the TTB structure by the rare-earth ions introduced inside the square channels. Studies of the $Ba_2RENb_3Ti_2O_{15}$ (RE = rare-earth atom) compounds containing trivalent ions such as Bi^{3+}, La^{3+}, Nd^{3+}, Sm^{3+}, and Gd^{3+}[52–55] demonstrated that both Bi- and La-based compounds exhibit relaxor behavior, whereas Nd-, Sm-, and Gd-based analogs are classical ferroelectrics. In $Ba_2RENb_3Ti_2O_{15}$ compounds, deviations from the ideal TTB symmetry caused by an incommensurate modulation was associated with relaxor behavior, whereas a commensurate modulation was observed for phases exhibiting ferroelectric behavior.[56–60] The above examples demonstrate the intricate relationships between the composition, structure, and properties of TTB systems, which were illustrated in an original way by the study of $Ba_2REFeNb_4O_{15}$ composite multiferroic ceramics.[61] At room temperature, the crystal structure of $Ba_2REFeNb_4O_{15}$ was described in a "pseudotetragonal" symmetry, space group *Pba*2 (no. 32), with $a \approx b = 12.514(1)$ Å and $c = 3.941(1)$ Å, and there was suspicion of the existence of structural modulations.[61] The $Ba_2REFeNb_4O_{15}$ family also shows an interesting correlation between structural and dielectric properties, which depends on the size of rare-earth cations. An uncommon evolution from ferroelectric to relaxor properties was found in the related solid solution $Ba_2Pr_xNd_{1−x}FeNb_4O_{15}$.[62] The accommodation of rare-earth ions in the square channels of the TTB framework appears to be the critical parameter that governs these dielectric behaviors. Indeed, a distortion of the octahedral framework is observed and is especially significant for the ferroelectric representatives (RE = Nd, Sm, Eu; Figure 1).
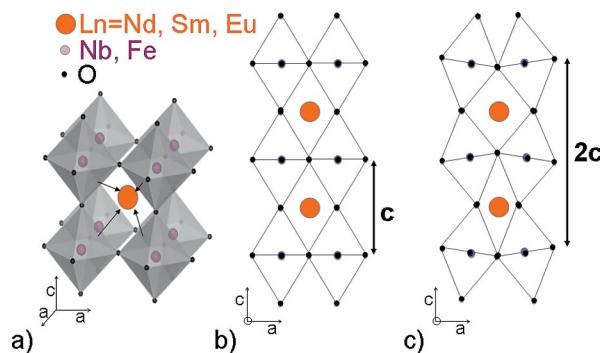

Figure 1. (a) Crystal structure of TTB that shows the small rare-earth cations inside the square channels surrounded by oxygen octahedra and the direction of the displacement of these octahedra. Schematic representations of (b) two layers of octahedra along the *c* axis in the commensurate TTB matrix and (c) the octahedral tiltings along the *c* axis induced by the rare-earth ion inside the square sites for the TTB matrix, which results in a doubling of the *c* parameter.

In these rare-earth substituted TTB compounds, and more specifically in the $Ba_2REFeNb_4O_{15}$ family, single crystals are necessary for investigation of the intrinsic physical and structural properties as well as their anisotropy. Focusing on these objectives, the high-temperature solution growth of $Ba_2REFeNb_4O_{15}$ (with RE = La, Pr, Nd, Sm, and Eu) has been undertaken and has already allowed the identification of a successful growth strategy.[63] However, in these initial experiments, the evaporation of the $LiBO_2$ flux impeded the growth of centimeter-sized single crystals and altered the quality of the as-grown crystals as well as their chemical homogeneity within the same batch. Hence, the optimization of the crystal growth process is of great importance, especially the inhibition of the flux volatilization under a controlled atmosphere by using a sealed platinum assembly crucible to obtain chemically and crystallographically homogeneous crystals. In addition, temperature cycling during the growth process and the approximate determination of $T_{solidus}$ allowed centimeter-sized crystals to be obtained.

This work focuses on the lanthanum-based compound, namely, $Ba_2LaFeNb_4O_{15}$ (BLFNO), which is considered as the prototype of the $Ba_2REFeNb_4O_{15}$ family. Following preliminary experiments that gave essential insight into the 30/70 mol-% region of the BLFNO–$LiBO_2$ phase diagram,[63] we present the optimized growth conditions that led to centimeter-sized BLFNO single crystals. Their chemical, physical, and structural properties were investigated by means of electron probe microanalysis/wavelength dispersive spectroscopy (EPMA/WDS) analysis, dielectric and magnetic measurements, and single-crystal X-ray diffraction.

Results and Discussion

The obtained BLFNO crystals were trapped in the remaining flux load and no weight loss of the assembly was detected. Single crystals ranging from millimeter to centi-

meter size grew within the whole load volume. Crystals with increasing size were actually spread from the bottom of the crucible to the surface of the load (Figure 2a). A centimeter-sized crystal (Figure 2b) was extracted and cut after orientation by means of the back-reflection X-ray Laue diffraction method (Figure 2c). An oriented crystal with final dimensions $3 \times 4 \times 5$ mm^3 was obtained with faces perpendicular to the [100], [010], and [001] crystallographic directions with an accuracy of about 1°.
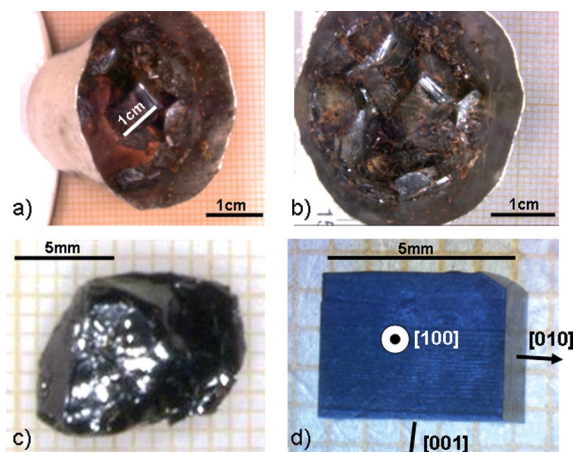

Figure 2. Centimeter-sized as-grown BLFNO crystals (a) partially trapped in the solidified flux and (b) following removal of the LiBO$_2$ flux. (c) As-grown BLFNO single crystal and (d) oriented single crystal showing the [100], [010], and [001] crystallographic axis.

Chemical Composition and XRD Analysis

EPMA performed on several crystals confirmed the formation of the TTB phase with uniform Ba$_2$La$_{0.9}$Fe$_{0.8}$Nb$_{4.2}$O$_{15}$ composition (Table 1). Small quantities of maghemite and fergusonite phases were also detected as side products by XRD. Their formation is consistent with a deviation from the stoichiometric composition Ba$_2$LaFeNb$_4$O$_{15}$ in the as-grown crystals. For this reason, special attention was paid to microprobe EPMA/WDS analysis, to check the homogeneity of both the crystals and the batch. In contrast with the crystals that were grown under uncontrolled atmosphere conditions, the endothermic flux volatilization of which entailed large thermal fluctuations at the liquid top, the as-grown crystals obtained here display a uniform black color and are devoid of composition variations. The growth conditions and control of the nucleation by temperature cycling have, thus, been optimized for the growth of centimeter-sized and chemically uniform BLFNO crystals.

Table 1. Chemical compositions of crystals determined by microprobe EPMA/WDS analysis.

Crystal	Composition
A	Ba$_{2.03(2)}$La$_{0.87(2)}$Fe$_{0.78(2)}$Nb$_{4.22(2)}$O$_{15.07(2)}$
B	Ba$_{2.03(2)}$La$_{0.88(2)}$Fe$_{0.77(2)}$Nb$_{4.23(2)}$O$_{15.08(2)}$
C	Ba$_{2.05(2)}$La$_{0.89(2)}$Fe$_{0.77(2)}$Nb$_{4.23(2)}$O$_{15.10(2)}$

The Ba$_{2.03(2)}$La$_{0.88(2)}$Fe$_{0.77(2)}$Nb$_{4.23(2)}$O$_{15.08(2)}$ formulation, obtained by considering a fully occupied octahedral framework, displays a readjusted Fe/Nb ratio, which compensates for the lanthanum losses and maintains electrical neutrality.

Dielectric Properties

The systematic faceting of the crystals suggests that the crystallographic face that has the slowest growth rate is the (001) face, which is perpendicular to the polarization direction. Indeed, in the TTB structure, the off-centering of niobium ions within the octahedra often induces dipolar moments that are oriented along the c axis. Therefore, this situation is highly favorable for dielectric characterization, because the measurement can be performed with electrodes perpendicular to the polarization direction. The (001) faces of the oriented crystal were sputtered with gold electrodes for dielectric measurements. The real and imaginary parts of the dielectric permittivity ε' and ε'' were then extracted for both measurements (Figure 3).
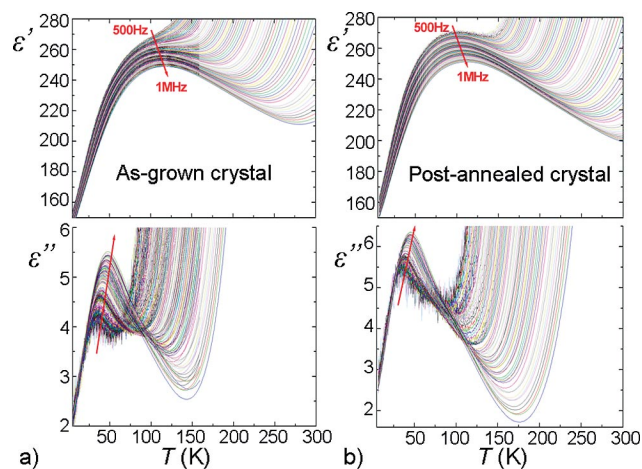

Figure 3. Variation of the real ε' and imaginary part ε'' of the complex dielectric permittivity of a BLFNO crystal, measured along [001] on heating from 5 to 300 K before (a) and after (b) postannealing at 900 °C under O$_2$.

The dielectric measurements revealed broad, frequency-dependent maxima in both the real and imaginary parts of the dielectric permittivity. Such features are characteristic of relaxor behavior. It is thus shown that our flux-grown, centimeter-sized BLFNO crystals exhibit a relaxor behavior similar to that observed in the corresponding ceramics.[64] Moreover, this result confirms that the relaxor behavior of BLFNO is an intrinsic response of the TTB framework.

However, contrary to what is observed in ceramics samples, a rapid increase of dielectric losses on heating of as-grown single crystals is observed and suggests the onset of electronic conduction in the crystal. As this conduction phenomenon was substantially reduced by post-annealing treatment in an oxidizing atmosphere, oxygen vacancies are likely to be involved. Oxygen vacancies can be created or suppressed by annealing in reducing (N$_2$) or oxidizing (O$_2$,

www.eurjic.org   **FULL PAPER**

air) atmospheres, respectively. The effect of such annealing conditions on the dielectric properties of oxides has been extensively reported.[65–69] In the case of our BLFNO crystals, it should be recalled that they were grown in a platinum assembly sealed under vacuum, that is, in a slightly reducing atmosphere. The growth conditions may thus favor the formation of oxygen vacancies in as-grown single crystals, the concentration of which is reduced upon annealing in an oxidizing atmosphere.

The transition temperature (T_m = 112 K at 1 MHz) and deviation temperature (T_d = 190 K at 1 MHz, deviation from Curie–Weiss behavior) after annealing are slightly different from the corresponding temperatures determined for the as-grown crystal (T_m = 118 K and T_d = 170 K at 1 MHz). These discrepancies in the T_m and T_d values of as-grown and annealed crystals may actually be related to the sensitivity of the TTB polar lattice to oxygen vacancies (as-grown vs. annealed). Beyond these variations of T_m and T_d, the relaxor behavior is retained in both as-grown and annealed crystals.

Magnetic Properties

Surprisingly, the magnetic susceptibility of BLFNO single crystals exhibits Curie–Weiss paramagnetic behavior over the 14–300 K temperature range. This is in great contrast with the magnetic susceptibility of BLFNO crystals reported in ref.[63] A negative Curie paramagnetic temperature θ_p = –17.4 K was obtained, which indicates antiferromagnetic (AFM) interactions between electronic spins. The effective magnetic moment in this compound is ca. 4.91 μ_B/Fe^{3+} ion, which is lower than the free ion effective magnetic moment $2[S(S + 1)]^{1/2}\mu_B \approx 5.92\ \mu_B$.

A deviation from the Curie–Weiss line appears at ca. 14 K (Figure 4a, inset) and is probably caused by the development of AFM correlations at low temperatures. In addition, although the $M(H)$ curve at 300 K is perfectly linear, the same curve at 4 K exhibits a slight S shape (Figure 4b). However, the ratio $\chi/\chi_{C-W} \approx 1.2$ remains very low down to 4.2 K.
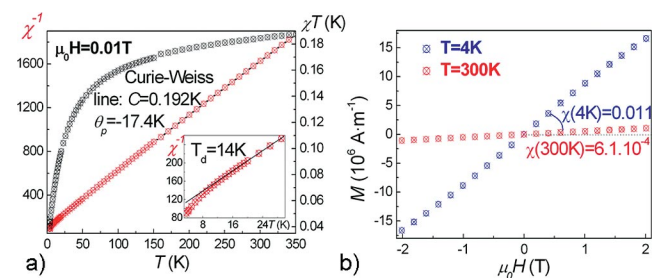

Figure 4. Magnetic measurements on crushed crystals. (a) Inverse of magnetic susceptibility vs. temperature from 2 K to room temp. (inset from 2 to 16 K) under 0.01 T displays the paramagnetic behavior of BLFNO single crystals, and the χT vs. T plot does not exhibit a minimum. (b) Magnetization at 4 and 300 K.

The absence of long-range magnetic order down to 4 K suggests that the AFM couplings are slightly frustrated. Taking into account that for a random distribution of Fe^{3+}

ions, which is supported by the Curie–Weiss behavior over an extended T range, the average distance between Fe^{3+} ions in is ca. $[3/(4\pi n_{Fe})]^{1/3} \approx 4.5$ Å, as least five different superexchange (SE) pathways can be recognized in this crystal structure.

In the simplest situation, the sign and magnitude of these couplings can be estimated by means of the Goodenough–Kanamori–Anderson (GKA) rules.[70] For example, these rules predict that (1) a 180° Fe–O–Fe coupling yields strong AFM exchange integrals (ca. 750 K, strong σ AFM overlapping and weak π AFM overlapping), (2) a 90° Fe–O–Fe coupling leads to moderate AF exchange integrals (ca. 200 K, σ and π AFM overlapping), and (3) a 180° Fe–O–O–Fe coupling results in weak AFM exchange integrals (ca. 75 K). The GKA rules also predict that for Fe–O–Fe angle values between approximately 125 and 150° an upturn in exchange spin should occur. On one hand, SE pathways such as Fe(1)–O(1)–Fe(1) (180°), Fe(2)–O(5)–Fe(2) (ca. 168°), and Fe(2)–O(3)–Fe(2) (ca. 171°) should lead to AFM couplings, which could explain the overall negative θ_p. The fact that the χT product decreases continuously down to 4.2 K (Figure 4a) without exhibiting any minimum suggests that SE paths such as Fe(1)–O(4)–Fe(2) (ca. 145°) and Fe(2)–O(2)–Fe(2) (ca. 140°), which could be ferromagnetic (FM), are negligible.

Crystal Structure

The space group, the lattice parameters and the modulation vectors were determined by investigation of two single crystals (with a Kappa CCD four circles diffractometer and an IPDS II STOE two circle diffractometer), which are referred to as crystal 1 and crystal 2, respectively. It was found that the Bravais lattice of the main structure is primitive and the extinction conditions are compatible with space group $P4/mbm$ (no.127). The evidence of structural modulation was found in several samples at room temperature, including crystal 1 and crystal 2. The reconstructed ($0kl$) and ($h0l$) precession photographs (crystal 1) revealed satellite reflections positioned exactly halfway between each row of main reflections along c^*, which indicates that the k_Z component of the modulation vector is 1/2.

The positions of the first-order satellite reflections observed in the ($hk0.5$) plane (Figure 5), with respect to their corresponding main reflections, can be indexed by a bidimensional modulation described by two modulation vectors $q_1 = (a, a, 1/2)$ and $q_2 = (a, –a, 1/2)$ with a = 0.295(1). The value of a is evidence that BLFNO single crystals adopt an incommensurately modulated crystal structure at room temperature. This bidimensional modulation is compatible with the $P4/mbm$ space group associated with the main reflections. This leads to a 5D crystal structure in the superspace formalism, which will be described elsewhere.

Refinements of the basic structures were performed in the space group $P4/mbm$ for both crystal 1 and crystal 2. Details of the data collection and refinement are summarized in Table 2, and the atomic parameters are listed in
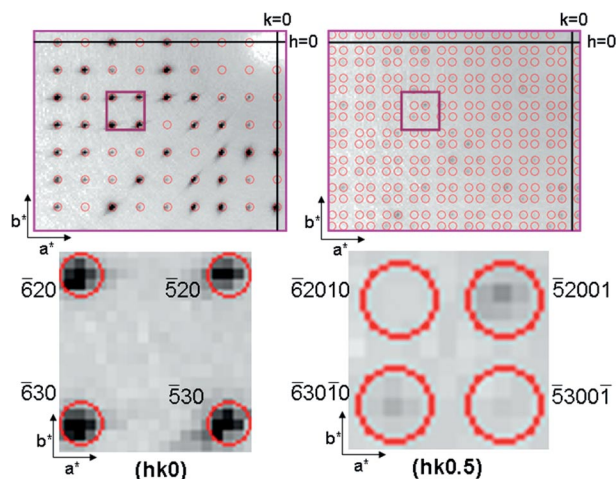
www.eurjic.org   **FULL PAPER**

Figure 5. Reconstructed image from observed BLFNO single-crystal data of the (*hk*0) (left) and (*hk*0.5) (right) planes with $hklq_1q_2$ indexations for some mean and satellite reflections, respectively.

Table 3. Restraints were introduced in the refinement to maintain electroneutrality and to force a full occupation of the octahedral framework.

Table 2. Crystal data and data collection and refinement details for crystals 1 and 2 (common characteristics of both crystals are gathered at the top of the table).

	$Ba_2La_{0.96(1)}Fe_{0.94(1)}Nb_{4.06(1)}O_{15}$ $M = 1081.01\,g\,mol^{-1}$ $\lambda = 0.71073$ Å, Mo-K_α, $T = 293(2)$ K tetragonal, $P4/mbm$, $Z = 2$	
	Crystal 1	Crystal 2
a [Å]	12.5202(2)	12.4942(18)
c [Å]	3.9364(1)	3.9406(8)
V [Å³]	617.05(2)	615.15(2)
$\rho_{calcd.}$ [g cm⁻³]	5.818	5.836
μ [mm⁻¹]	14.455	14.5
$F(000)$	958	958
Diffractometer	Nonius Kappa CCD	IPDS II STOE
Scan strategy	ω/ϕ	ϕ
$[\theta_{min}-\theta_{max}]$ [°]	[3.25–33.74]	[2.31–32]
Limiting indices	$-18 < h < 19$	$-18 < h < 18$
	$-19 < k < 19$	$-18 < k < 18$
	$-6 < l < 6$	$-5 < l < 5$
Measured reflections	6134	7423
Independent reflections	268	294
Reflections with $F_o > 4\sigma(F_o)$	695	625
Refinement program	SHELXL97	
$R[F^2 > 2\sigma(F^2)]$	0.0272	0.0312
$wR(F^2)$	0.0534	0.0641
S	1.176	1.461
Total reflections	715	628
Refinement parameter	49	49
Extinction coefficient	0.0138(6)	0.0129(7)
ρ_{min}/ρ_{max} [e Å⁻³]	–1.119/1.155	–1.632/1.627

Both refinements converged to satisfying agreement factors and comparable atomic positional and equivalent isotropic displacement parameters. The refined chemical compositions are identical but are significantly different from those extracted from EPMA characterization. However, one should keep in mind that these compositions are associ-

Table 3. Positional and equivalent isotropic displacement parameters for BLFNO crystals 1 and 2.

Atom	Position	x	y	z	U_{eq} [Å²]	Occupancy
Crystal 1: $Ba_2La_{0.96(1)}Fe_{0.94(1)}Nb_{4.06(1)}O_{15}$						
Ba1	8j	0.3392(1)	0.1797(1)	0.5	0.0151(4)	0.5
La1	2b	0	0	0.5	0.0091(2)	0.96(1)
Fe1	2d	0.5	0	0	0.0141(2)	0.22(1)
Nb1	2d	0.5	0	0	0.0141(2)	0.78(1)
Fe2	8i	0.07482(4)	0.21511(4)	0	0.0081(2)	0.18(1)
Nb2	8i	0.07482(4)	0.21511(4)	0	0.0081(2)	0.82(1)
O1	2c	0.5	0	0.5	0.031(2)	1
O2	4g	0.2185(3)	0.2815(3)	0	0.0134(10)	1
O3	8i	0.1335(4)	0.0655(3)	0	0.0308(12)	1
O4	8i	0.3430(3)	0.0070(3)	0	0.0226(9)	1
O5	8j	0.0763(6)	0.1983(5)	0.5	0.040(2)	1
Crystal 2: $Ba_2La_{0.96(1)}Fe_{0.94(1)}Nb_{4.06(1)}O_{15}$						
Ba1	8j	0.3382(3)	0.1792(3)	0.5	0.0134(7)	0.5
La1	2b	0	0	0.5	0.0065(2)	0.96(1)
Fe1	2d	0.5	0	0	0.0112(3)	0.18(1)
Nb1	2d	0.5	0	0	0.0112(3)	0.82(1)
Fe2	8i	0.07479(5)	0.21490(5)	0	0.0059(2)	0.19(1)
Nb2	8i	0.07479(5)	0.21490(5)	0	0.0059(2)	0.81(1)
O1	2c	0.5	0	0.5	0.026(3)	1
O2	4g	0.2190(4)	0.2810(4)	0	0.0100(13)	1
O3	8i	0.1332(5)	0.0661(5)	0	0.0288(16)	1
O4	8i	0.3427(4)	0.0070(4)	0	0.0191(12)	1
O5	8j	0.0748(8)	0.1992(6)	0.5	0.038(2)	1

ated with an incomplete structural model that does not take into account the bidimensional modulation that affects the TTB framework. The nature of this modulation (positional, occupational or both) may affect the overall composition as evaluated by crystallographic means.

In the refined crystal structures, the barium sites within the pentagonal channels are fully occupied. The O2, O3, and O4 atoms, which form the equatorial square of the NbO_6 octahedra associated with the Nb(2) site, display octahedral distortion with small variations of the Nb–O distances and changes of the intra-octahedral O–Nb–O angles ranging from 81.23 to 97.81° (Figure 6a). Owing to its symmetry, the Nb(1)site (Wyckoff position 2d) is not affected by such distortions, and the cation–oxygen lengths are equivalent for this regular octahedron (Figure 6b). The distortions affecting the Nb(2) site result in slight shifts of the centers of negative charges, so small dipolar moments located in the (*ab*) plane are present in BLFNO single crystals at room temperature. The absence of a macroscopic spontaneous polarization, as demonstrated by dielectric measurements would then be due to the fourfold symmetry axis located at the center of the square channels, as it implies a perfect compensation of in-plane dipolar moments. In the basic structure, this situation could be compatible with an antiferroelectric state, although the actual polar state of the sample should account for the structural modifications associated with the incommensurate modulation. These may, for example, either hinder the full compensation of in-plane dipolar moments to yield ferrielectric behavior or suppress the distortions at the origin of the in-plane dipolar moments. It should be noted that in-plane dipolar moments

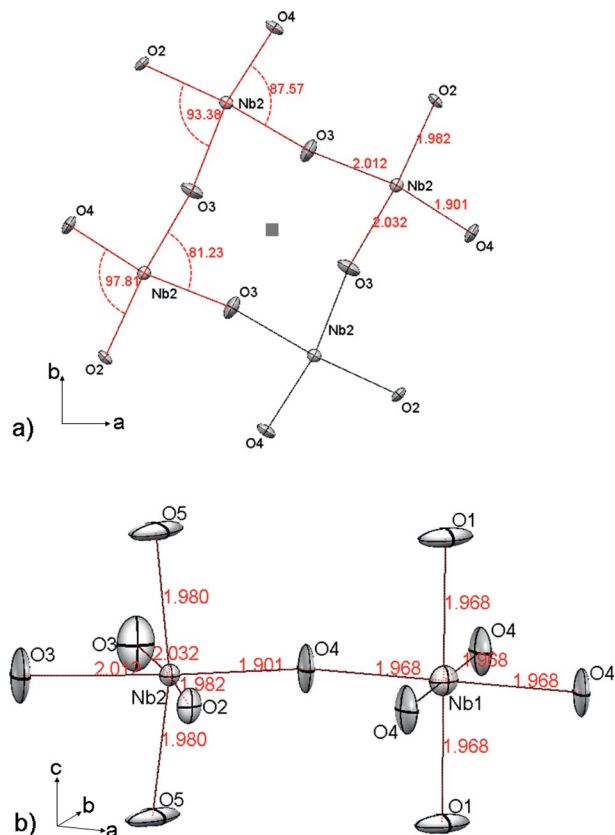have been observed in some lead-containing TTB ferroelectrics.[71]

Figure 6. ORTEP drawings at 50% probability level with atom labeling. O–Nb–O distortion angle [°] and Nb–O bond length [Å] reported (a) along the (ab) plane for the square channel containing La^{3+} ions (not represented) and (b) for local oxygen environments for Nb1/Fe1 and Nb2/Fe2 cations in their respective octahedral sites.

The atomic displacements ellipsoids of the O atoms are anomalously elongated in the basic structure, either perpendicular (O1 and O5) or parallel (O2, O3, and O4) to the tetragonal c axis (Figure 6b). This suggests that the large atomic displacement parameters of the anionic framework in the basic structure encompass a static contribution from displacive modulations, in addition to the thermal vibrations of the atoms. The atomic displacement ellipsoids of the O atoms are similar to those reported for calcium barium nitrate (CBN).[50]

These modulations are likely to play a role in the dielectric behavior of BLFNO crystals. Furthermore, the modification of T_m and T_d by post-annealing under oxygen shows that the dielectric properties are sensitive to oxygen vacancies. Thus, one may expect that oxygen vacancies may also affect the aperiodic modulation that takes place in the anionic framework. Correlations between defects and structural and dielectric properties in TTB have been previously investigated,[72] however, determination of such correlations in BLFNO first require a thorough study of the 5D modulated structure.

In our early studies of the Ba$_2$REFeNb$_4$O$_{15}$ (BREFNO) family,[61] we envisaged the existence of such aperiodic features. However, we did not actually expect them in the lanthanum representative, which is paraelectric at room temperature, as we supposed they were related to the ferroelectric state. Thus, the present observations, and the possible existence of in-plane dipolar moments associated with a ferri- or antiferroelectric state, may help us to understand some overlooked aspects of the crystal chemistry of TTB ferroelectrics.

Conclusions

Centimeter-sized BLFNO single crystals have been grown by a high-temperature solution growth method under optimized conditions (sealed platinum assembly, thermal cycle). Direct observation of the solidus was possible following a preliminary experiment, thanks to the use of an inverted thermal gradient, which could prove useful for the exploration of growth conditions. A combination of EPMA/WDS analysis, dielectric and magnetic characterizations, and single-crystal XRD analysis firmly established that the high-temperature solution growth process allows for the growth of higher quality, centimeter-sized, chemically and structurally homogeneous BLFNO crystals. This process should prove fruitful for the growth of other representatives of the BREFNO family and could probably be used to grow others niobates for which molten-state growth methods are inadequate.

The chemical, structural, and physical properties of BLFNO crystals are preserved with respect to the corresponding polycrystals. A slight modification of the chemical composition, consistent with the behavior observed in polycrystalline Ba$_2$REFeNb$_4$O$_{15}$ samples, was detected from EPMA, XRD, and magnetic properties studies. The relaxor behavior of BLFNO crystals was confirmed. In contrast with previous studies, paramagnetic behavior was observed for BLFNO crystals down to 14K, a temperature below which a deviation from Curie–Weiss behavior was observed because of AFM interactions. An incommensurately modulated structure was revealed in BLFNO single crystals at room temperature. The modulation vectors can be expressed as $q_1 = (a, a, 1/2)$ and $q_2 = (a, -a, 1/2)$ with $a = 0.295(1)$. Refinement of the basic structure revealed the possible existence of in-plane dipolar moments, which should be confirmed by further investigations dedicated to the description of the crystal structure as a 5D aperiodic crystal in superspace formalism.

These results and the ability to grow centimeter-sized single crystals offer promising perspectives for the crystal chemical understanding of TTB structured materials.

Experimental Section

Synthesis: The synthesis of BLFNO powders was performed by a conventional solid-state reaction. High purity starting reagents, barium carbonate BaCO$_3$ (Cerac, 99.9%), lanthanum oxide La$_2$O$_3$

(Cerac, 99.99%), iron oxide Fe_2O_3 (Rectapur, 99%), and niobium oxide Nb_2O_5 (LTS chemical, 99.95%), were used. La_2O_3 was first dried at 900 °C for 10h to remove hydroxy groups and then mixed with other oxides and carbonate in stoichiometric proportions by ball-milling (agate balls and mortar) in ethanol for 1h30 with an alternated rotation (every 15 minutes) at 500 rpm. The mixture was then heated to 1280 °C for 12h to obtain the TTB phase, which was confirmed by powder XRD analysis at room temperature. The data were fully indexed with a TTB unit cell, and there was no evidence of secondary phases.

30/70 mol-% Region of the BLFNO–LiBO₂ Phase Diagram Investigated for Crystal Growth: As demonstrated by Castel et al.,[63] the growth of single crystals of BLFNO requires precise control of the growth conditions to obtain chemically homogeneous TTB crystals. In this first study, growth attempts were undertaken in a top-open platinum crucible under air, and the volatilization of the $LiBO_2$ flux proved to be an important and uncontrolled growth parameter. Several growth attempts have shown a high rate of nucleation of BLFNO crystals with a high volatilization rate of the flux. This was detrimental to the growth of crystals with dimensions larger than a few millimeters. Moreover, crystals analysis highlighted substantial variations of the crystals composition as well as different crystallographic structures.

In the present work, we aimed to understand the 30/70 mol-% region of the BLFNO–LiBO₂ phase diagram in the temperature range 850–1330 °C, which was previously investigated for the growth of BLFNO crystals.[63] BLFNO flux growth under a controlled atmosphere was achieved for the first time. $LiBO_2$ was chosen as solvent with a BLFNO/LiBO₂ molar ratio of 3:7, as previously determined.[63] BLFNO and $LiBO_2$ powders were mixed together by dry ball-milling for 1h, and the final mixture was compacted into 1 cm high and 1 cm diameter pellets. A platinum crucible was loaded with BLFNO–LiBO₂ mixture (20g) in the form of powder and pellets (Figure 7). To minimize the volatilization of the solution during the growth and with the assumption that the $LiBO_2$ vapor pressure at ca. 1300 °C ranges from 10^{-3} to 10^2 atm,[73–75] the crucible was then placed in a platinum chamber. This external Pt chamber was sealed under primary vacuum (4×10^{-3} mbar) in such a way as to avoid buckling during the thermal process.
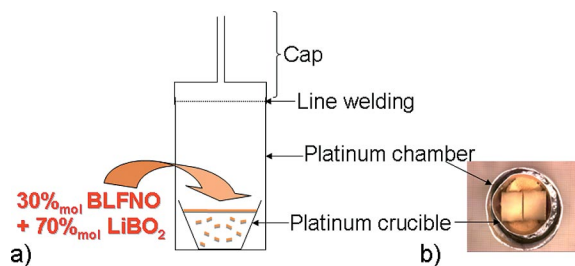

Figure 7. (a) Schematic drawing of the Pt chamber assembly closed with a Pt cap that contains an inner platinum crucible loaded with BLNFO–LiBO₂ powder mixture. (b) Top view of crucible and chamber assembly used for high-temperature solution growth of BLNFO.

The Pt crucible and chamber assembly was placed into a vertical resistive furnace with a 3 °Ccm⁻¹ axial thermal gradient. This thermal configuration was designed to initiate the crystal growth and remove the latent heat of crystallization at the bottom of the inner crucible. Thus, this would allow us to overcome the thermal fluctuations at the top of the liquid that are likely to be induced by the endothermic and unsteady flux volatilization.

Two growth attempts were performed. In experiments 1 and 2, the temperature was increased to 1273 and 1323 °C, respectively, with a dwelling time of 24h. The solutions were cooled to 850 °C at a rate of 1 °Ch⁻¹. Finally, the last part of the growth was monitored with a –30 °Ch⁻¹ temperature slope down to room temperature.

The first and second growths led to as-grown BLFNO crystals with average sizes of 3 and 6 mm, respectively (Figures 8 and S1). No weight loss for the whole Pt assembly was measured, which proves that $LiBO_2$ volatilization was successfully controlled by means of this new set-up. Consequently, the control of the supersaturation of the solution was made possible by exclusive variation of the temperature of the Pt assembly and, thus, more steady crystal growth could be performed than that for previous experiments with top-open crucibles.[63]
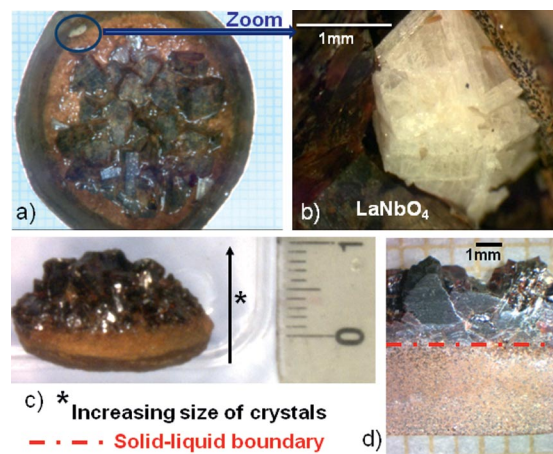

Figure 8. Experiment 1: (a) As-grown BLFNO singles crystals located at the top of the solidified solution. (b) Millimetric $LaNbO_4$ parasitic crystal formed by partial BLFNO decomposition during the growth. (c) View of the bottom part of extracted solidified solution after growth. (d) The solid–liquid boundary corresponding to the solidus temperature (1275 °C) in the 30/70 mol-% region of the BLFNO–LiBO₂ phase diagram was clearly evident.

After removal of the $LiBO_2$ flux from samples by dilution in HCl for several hours, powder XRD measurements confirmed the crystallization of the BLFNO phase and two secondary phases (Figure S2), ferrimagnetic maghemite γ-Fe_2O_3 (ICDD 39–1346) and fergusonite $LaNbO_4$ (ICDD 22–1125). During both growth runs, crystals of $LaNbO_4$ were obtained as a side product (Figures 8b and S1a). In experiment 2, numerous and large white crystals of $LaNbO_4$ were obtained, whereas experiment 1 yielded fewer and smaller $LaNbO_4$ crystals. Few details can be found in the literature about single-crystalline $LnNbO_4$ lanthanide orthoniobates. They adopt the fergusonite structure and can display luminescent properties[76–77] and a ferroelastic transition.[78] Apart from a single-crystal structural study in 1977 by Tsunekawa et al.[79] and crystal growth by the Czochralski method,[80] previously investigated $LnNbO_4$ crystals were prepared by flux growth methods,[81–83] and Octaviano[84] recently reported the use of the floating-zone method at 1300 °C. Our experiments thus show that the BLFNO phase grown in $LiBO_2$ flux is not the only stable phase over the 850–1330 °C temperature range. This suggests that BLFNO could exhibit an incongruent behavior, which may lead to a different stoichiometry of the BLFNO single crystal than the one expected from the initial BLFNO solute.

In addition, the nucleation rate of the BLFNO crystals was found to be slightly higher during the first experiment, in which the load

was not completely molten. According to the thermal gradient set (measured without Pt chamber assembly) in the vicinity of the solid–liquid boundary observed in Figure 3d, the solidus temperature was found to be around 1275 °C for the 30/70 mol-% BLFNO–$LiBO_2$ mixture. Above this temperature (i.e., at higher heights in our assembly), we observed that the nucleation and growth of numerous BLFNO single crystals increases as their location lies closer to the surface of the load. Although experiment 2 has shown a complete melting of the load, which led to the growth of larger BLFNO crystals and numerous crystals of secondary phases, experiment 1 led to smaller BLNFO crystals and a lower proportion of smaller $LaNbO_4$ crystals. An attempt to grow large-sized crystals of BLNFO with low formation rates of γ-Fe_2O_3 and $LaNbO_4$ phases was considered and is presented in the following.

Large-Sized BLFNO Crystal Growth: As previously described, a 30/70 mol-% BLFNO–$LiBO_2$ mixture (20 g) was used. The assembly used previously was placed into a vertical resistive furnace with a lower inverted thermal gradient $G = 0.5$ °C cm^{-1}. The chamber was then sealed under primary vacuum (4×10^{-3} mbar). The growth temperature was set to 1293 °C, which is intermediate between the temperatures investigated in the previous experiments. The cooling rate was reduced to make the crystal growth process steadier. The classical way of growing crystals from solutions, which presents a high probability of polynucleation rate, as widely described by Elwell and Scheel,[85] was carried out and is described in Figure 9. It consisted of: (1) Thermal homogenization of the solution with a 24h dwelling time at 1293 °C. (2) A first crystals growth step with a –0.4 °C h^{-1} temperature slope down to 1261 °C. (3) Dissolution of the smaller grown crystals by fast heating of the solution to 1278 °C. (4) A second crystals growth step with a –0.2 °C h^{-1} temperature slope down to 1223 °C to enlarge the remaining largest crystals formed during the first growth step.
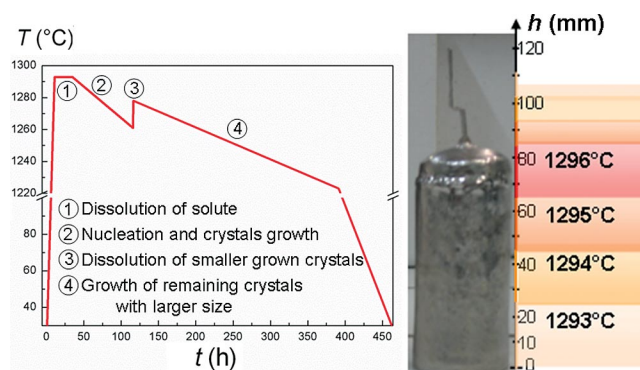

Figure 9. Thermal treatment applied for the BLFNO growth (left) and measured thermal profile in the Pt assembly (right).

The system was finally cooled to room temperature at a rate of –30 °C h^{-1}. No rotation of the crucible was set, so that crystal growth was only affected by buoyancy-driven convective motions and chemical diffusion of species within the solution.

Physical and Structural Characterizations of Large-Sized BLFNO Crystals: Capacitance and dielectric losses were measured from 500 Hz to 1 MHz on heating from 5 to 300K. The measurements were performed first on an as-grown BLFNO crystal and then on the same crystal post-annealed at 900 °C for 3 h under O_2 atmosphere. The magnetic susceptibility of crushed crystals was measured with a superconducting quantum interference device (SQUID) magnetometer at 2–300 K and under an applied magnetic field of 0.1 T. Single-crystal XRD analysis was performed with a

Kappa CCD four circle diffractometer at ICMCB, Université de Bordeaux, and with an IPDS II STOE two circle diffractometer at the Laboratoire de Cristallographie, Ecole Polytechnique Fédérale de Lausanne, both with monochromatized Mo-K_α radiation. The crystal structure was refined with SHELXL97[86] by using the WINGX32 software package.[87]

Supporting Information (see footnote on the first page of this article): Details of EPMA on large-sized BLFNO single crystals. Powder XRD patterns and images of crystals grown in experiment 2.

Acknowledgments

[1] P. A. Ramakrishnan, S. Sampath, G. V. Subba Rao, *Mater. Chem. Phys.* **1993**, *34*, 295–299.
[2] P. R. Slater, J. T. S. Irvine, *Solid State Ionics* **1999**, *124*, 61–72.
[3] P. R. Slater, J. T. S. Irvine, *Solid State Ionics* **1999**, *120*, 125–134.
[4] A. Kaiser, J. L. Bradley, P. R. Slater, J. T. S. Irvine, *Solid State Ionics* **2000**, *135*, 519–524.
[5] E. Kendrick, M. S. Islam, P. R. Slater, *Solid State Ionics* **2005**, *176*, 2975–2978.
[6] L. E. Cross, *Ferroelectrics* **1994**, *151*, 305–320.
[7] A. Simon, J. Ravez, *C. R. Chim.* **2006**, *9*, 1268–1276.
[8] J. J. Rubin, L. G. Van Uitert, H. J. Levinstein, *J. Cryst. Growth* **1967**, *1*, 315–317.
[9] L. G. Van Uitert, J. J. Rubin, W. A. Bonner, *I. E. E. E. J. Quant. Electr.* **1968**, 622–626.
[10] R. Zupp, J. W. Nielsen, P. Vittorio, *J. Cryst. Growth* **1969**, *5*, 269–273.
[11] B. A. Scott, E. A. Giess, D. F. O'Kane, *Mater. Res. Bull.* **1969**, *4*, 107–117.
[12] S. Singh, D. A. Draegert, J. E. Geusic, *Phys. Rev. B* **1970**, *2*, 2709–2724.
[13] K. G. Barraclough, I. R. Harris, B. Cockayne, J. G. Plant, A. W. Vere, *J. Mater. Sci.* **1970**, *5*, 389–393.
[14] A. A. Ballman, J. R. Carruthers, H. M. O'Bryan, *J. Cryst. Growth* **1970**, *6*, 184–186.
[15] A. A. Ballman, S. K. Kurtz, H. Brown, *J. Cryst. Growth* **1971**, *10*, 185–189.
[16] A. A. Kaminskii, V. A. Koptsik, Y. A. Maskaev, I. I. Naumova, L. N. Rashkovich, S. E. Sarkisov, *Phys. Status Solidi A* **1975**, *28*, K5–K10.
[17] H. D. Quandt, L. R. Rothrock, *J. Cryst. Growth* **1977**, *42*, 435–439.
[18] M. Tsukioka, S. Kuroiwa, M. Tanokura, M. Kobayashi, M. Shimazu, S. Tsutsumi, *Mod. Phys. Lett. B* **1990**, *4*, 1017–1021.
[19] M. Shimazu, M. Tsukioka, S. Kuroiwa, Y. Tanokura, S. Tsutsumi, *Jpn. J. Appl. Phys.* **1991**, *30*, 2002–2007.
[20] M. Tsukioka, T. Fujimoto, S. Tsutsumi, *Mod. Phys. Lett. B* **1994**, *8*, 785–798.
[21] H. R. Xia, L. J. Hu, C. J. Wang, L. X. Li, S. B. Yue, X. L. Mang, L. Zhu, Z. H. Yang, J. Y. Wang, *J. Appl. Phys.* **1998**, *83*, 2560–2562.
[22] H. R. Xia, L. X. Li, H. Yu, X. L. Meng, L. Zhu, L. J. Hu, *Cryst. Res. Technol.* **1999**, *34*, 901–910.
[23] J. J. Romero, A. Brenier, L. E. Bausa, G. Boulon, J. Garcia Solé, A. A. Kaminskii, *Opt. Commun.* **2001**, *191*, 371–375.
[24] J. S. Abell, K. G. Barraclough, I. R. Harris, A. W. Vere, B. Cockayne, *J. Mater. Sci.* **1971**, *6*, 1084–1092.
[25] G. Foulon, M. Ferriol, A. Brenier, G. Boulon, *Eur. J. Solid State Inorg. Chem.* **1996**, *33*, 673–686.

[26] G. Foulon, A. Brenier, M. Ferriol, M. T. Cohen-Adad, G. Boulon, *Chem. Phys. Lett.* **1996**, *249*, 381–386.

[27] G. Foulon, A. Brenier, M. Ferriol, M. T. Cohen-Adad, G. Boulon, *J. Lumin.* **1997**, *72574*, 794–796.

[28] M. Ferriol, G. Foulon, A. Brenier, G. Boulon, *J. Mater. Sci.* **1998**, *33*, 1227–1232.

[29] F. Carrillo Romo, C. Goutaudier, Y. Guyot, M. T. Cohen-Adad, G. Boulon, K. Lebbou, A. Yoshikawa, T. Fukuda, *Opt. Mater.* **2001**, *16*, 199–206.

[30] M. Shimazu, M. Tsukioka, N. Mitobe, S. Kuroiwa, S. Tsutsumi, *J. Mater. Sci.* **1990**, *25*, 4525–4530.

[31] K. Lebbou, V. I. Chani, A. Yoshikawa, K. Shimamura, T. Fukuda, M. T. Cohen-Adad, A. Brenier, G. Boulon, M. Ferriol, *Mater. Res. Bull.* **2000**, *35*, 1277–1284.

[32] K. Lebbou, H. Itagaki, A. Yoshikawa, T. Fukuda, F. Carillo-Romo, G. Boulon, A. Brenier, M. T. Cohen-Adad, *J. Cryst. Growth* **2000**, *210*, 655–662.

[33] K. Lebbou, H. Itagaki, A. Yoshikawa, T. Fukuda, G. Boulon, A. Brenier, *J. Cryst. Growth* **2001**, *224*, 59–66.

[34] S. Bigotta, G. Gorini, A. Toncelli, M. Tonelli, E. Cavalli, E. Bovero, *Opt. Mater.* **2006**, *28*, 395–400.

[35] S. Bigotta, A. Toncelli, M. Tonelli, E. Cavalli, E. Bovero, *Opt. Mater.* **2007**, *30*, 129–131.

[36] E. Cavalli, A. Belletti, R. Mahiou, P. Boutinaud, *J. Lumin.* **2010**, *130*, 733–736.

[37] M. E. Lines, A. M. Glass, *Principles and Applications of Ferroelectrics and Related Materials*, Oxford University Press, UK, **2001**, pp. 280–292.

[38] S. H. Wemple, M. DiDomenico, I. Camlibel, *Appl. Phys. Lett.* **1968**, *12*, 209–211.

[39] L. G. Van Uitert, H. J. Levinstein, J. J. Rubin, C. D. Capio, E. F. Dearborn, W. A. Bonner, *Mater. Res. Bull.* **1968**, *3*, 47–58.

[40] P. B. Jamieson, S. C. Abrahams, J. L. Bernstein, *J. Chem. Phys.* **1969**, *50*, 4352–4363.

[41] L. G. Van Uitert, J. J. Rubin, W. H. Grodkiewicz, W. A. Bonner, *Mater. Res. Bull.* **1969**, *4*, 63–73.

[42] P. B. Jamieson, S. C. Abrahams, J. L. Bernstein, *J. Chem. Phys.* **1968**, *48*, 5048–5057.

[43] T. S. Chang, E. Amzallag, M. Rokni, *Ferroelectrics* **1971**, *3*, 57–58.

[44] J. Schneck, J. C. Toledano, G. Errandonea, A. Litzler, H. Savary, C. Manolikas, J. M. Kiat, G. Calvarin, *Phase Transitions* **1987**, *9*, 359–364.

[45] P. Labbe, H. Leligny, B. Raveau, J. Schneck, J. C. Toledano, *J. Phys. Condens. Matter* **1990**, *2*, 25–43.

[46] J. C. Toledano, *Phys. Rev. B* **1975**, *12*, 943–950.

[47] J. Schneck, F. Denoyer, *Phys. Rev. B* **1981**, *23*, 383–388.

[48] A. Simon, G. T. Joo, M. Maglione, J. Ravez, *Solid State Sci.* **2007**, *9*, 52–56.

[49] T. Woike, V. Petricek, M. Dusek, N. K. Hansen, P. Fertey, C. Lecomte, A. Arakcheeva, G. Chapuis, M. Imlau, R. Pankrath, *Acta Crystallogr. Sect. B* **2003**, *59*, 28–35.

[50] H. A. Graetsch, C. S. Pandey, J. Schreuer, M. Burianek, M. Mühlberg, *Acta Crystallogr. Sect. B* **2012**, *68*, 101–106.

[51] H. A. Graetsch, J. Schreuer, M. Burianek, M. Mühlberg, *J. Solid State Chem.* **2012**, *196*, 255–266.

[52] X. H. Zheng, X. M. Chen, *J. Mater. Res.* **2002**, *17*, 1664–1670.

[53] X. H. Zheng, X. M. Chen, *Solid State Commun.* **2003**, *125*, 449–454.

[54] G. C. Miles, M. C. Stennett, I. M. Reaney, A. R. West, *J. Mater. Chem.* **2005**, *15*, 798–802.

[55] S. Kamba, S. Veljko, M. Kempa, M. Savinov, V. Bovtun, P. Vanek, J. Petzelt, M. C. Stennett, I. M. Reaney, A. R. West, *J. Eur. Ceram. Soc.* **2005**, *25*, 3069–3073.

[56] M. C. Stennett, G. C. Miles, J. Sharman, I. M. Reaney, A. R. West, *J. Eur. Ceram. Soc.* **2005**, *25*, 2471–2475.

[57] I. Levin, M. C. Stennett, G. C. Miles, D. I. Woodward, A. R. West, I. M. Reaney, *Appl. Phys. Lett.* **2006**, *89*, 122908.

[58] M. C. Stennett, I. M. Reaney, G. C. Miles, D. I. Woodward, A. R. West, C. A. Kirk, I. Levin, *J. Appl. Phys.* **2007**, *101*, 104114.

[59] M. Prades, H. Beltrán, N. Masó, E. Cordoncillo, A. R. West, *J. Appl. Phys.* **2008**, *104*, 104118.

[60] X. L. Zhu, X. M. Chen, X. Q. Liu, X. G. Li, *J. Appl. Phys.* **2009**, *105*, 124110.

[61] M. Josse, O. Bidault, F. Roulland, E. Castel, A. Simon, D. Michau, R. Von der Mühll, O. Nguyen, M. Maglione, *Solid State Sci.* **2009**, *11*, 1118–1123.

[62] E. Castel, M. Josse, D. Michau, M. Maglione, *J. Phys. Condens. Matter* **2009**, *21*, 452201.

[63] E. Castel, P. Veber, M. Albino, M. Velázquez, S. Pechev, D. Denux, J. P. Chaminade, M. Maglione, M. Josse, *J. Cryst. Growth* **2012**, *340*, 156–165.

[64] E. Castel, *Synthèse de nouveaux matériaux multiferroïques au sein de la famille des bronzes quadratiques de formule Ba₂LnFeNb₄O₁₅*, Ph. D. Thesis, University Bordeaux 1, **2009**, pp. 109–111.

[65] O. Bidault, P. Goux, M. Kichikech, M. Belkaoumi, M. Maglione, *Phys. Rev. B* **1994**, *49*, 7868–7873.

[66] A. Chen, Y. Zhi, L. E. Cross, *Phys. Rev. B* **2000**, *62*, 228–236.

[67] N. Vittayakorn, S. Uttiya, G. Rujijanagul, D. P. Cann, *J. Phys. D: Appl. Phys.* **2005**, *38*, 2942–2946.

[68] P. Goel, K. L. Yadav, *Mater. Lett.* **2006**, *60*, 3183–3187.

[69] J. Bubesh Babu, G. Madeswaran, X. L. Chen, R. Dhanasekaran, *Mater. Sci. Eng. B* **2009**, *156*, 36–41.

[70] J. B. Goodenough, *Magnetism and chemical bond*, Interscience-Wiley, New York, **1963**, pp. 165–185.

[71] P. Sciau, G. Calvarin, J. Ravez, *Acta Crystallogr. Sect. B* **1999**, *55*, 459–466.

[72] G. Errandonea, J. Schneck, J. C. Toledano, A. Litzler, H. Savary, J. Aubree, J. M. Kiat, G. Calvarin, *Ferroelectrics* **1984**, *53*, 247–250.

[73] L. W. Zhang, M. Kobayashi, K. Goto, *Solid State Ionics* **1986**, *18–19*, 741–746.

[74] D. L. Hildenbrand, L. P Thoard, N. D. Potter, *An experimental program for obtaining the thermodynamic properties of propellant combustion products*, Third quarterly technical summary report, Defense Technical Information Center, AD273792, **1962**, pp. 13–14.

[75] C. Julien, G. A. Nazri, *Solid state batteries: Materials design and optimization*, Kluwer Academic Publishers, Boston, **1994**.

[76] G. Blasse, A. Bril, *J. Lumin.* **1970**, *3*, 109–131.

[77] L. H. Brixner, G. Blasse, *Mater. Res. Bull.* **1990**, *25*, 1003–1010.

[78] Y. A. Teterin, T. N. Bondarenko, A. Y. Teterin, A. M. Lebedev, I. O. Utkin, *J. Electron Spectrosc. Relat. Phenom.* **1998**, *88–91*, 267–273.

[79] S. Tsunekawa, H. Takei, M. Ishigame, *Mater. Res. Bull.* **1977**, *12*, 1087–1094.

[80] S. Tsunekawa, H. Takei, *J. Cryst. Growth* **1977**, *38*, 55–60.

[81] G. M. Wolten, A. B. Chase, *Am. Mineral.* **1967**, *52*, 1536–1541.

[82] G. Garton, B. M. Wanklyn, *J. Mater. Sci.* **1968**, *3*, 395–401.

[83] G. Garton, S. H. Smith, B. M. Wanklyn, *J. Cryst. Growth* **1972**, *13/14*, 588–592.

[84] E. S. Octaviano, D. Reyes Ardila, L. H. C. Andrade, M. Siu Li, J. P. Andreeta, *Cryst. Res. Technol.* **2004**, *39*, 859–863.

[85] D. Elwell, H. J. Scheel, in: *Crystal Growth from High-Temperature Solutions*, Academic Press, London, **1975**.

[86] G. M. Sheldrick, *Acta Crystallogr. Sect. A* **2008**, *64*, 112–122.

[87] L. J. Farrugia, *J. Appl. Crystallogr.* **1999**, *32*, 837–838.

Received: January 4, 2013
Published Online: ■

Solid-State Structures

**M. Albino, P. Veber, E. Castel,
M. Velázquez, K. Schenk, G. Chapuis,
M. Lahaye, S. Pechev, M. Maglione,
M. Josse*** **1–10**

Growth and Characterization of Centimeter-Sized $Ba_2LaFeNb_4O_{15}$ Crystals from High-Temperature Solution under a Controlled Atmosphere

Keywords: Crystal growth / Solid-state structures / Flux methods / Barium / Niobium / Relaxors
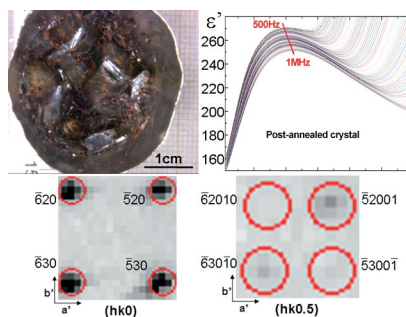
Centimeter-sized $Ba_2LaFeNb_4O_{15}$ (BLFNO) crystals are obtained by a flux method. A frequency-dependent dielectric permittivity maximum is found ($T_m = 100$ K at 5 kHz), which indicates relaxor behavior. Single-crystal XRD analysis reveals an incommensurate structure at room temperature with a bidimensional modulation characterized by vectors $q_1 = (a, a, 1/2)$ and $q_2 = (a, -a, 1/2)$ with $a = 0.295(1)$.